Atmósfera 39, 169-187 (2025)
https://doi.org/10.20937/ATM.53407

A case study of the sea/land breeze diurnal cycle in the Peninsula and Gulf of Nicoya, Costa Rica: Interactions with local and regional processes

Natali MORA[1]*, Jorge A. AMADOR[1,2], Erick R. RIVERA[1,2] and Tito MALDONADO[1,2]

[1] *Centro de Investigaciones Geofísicas, Universidad de Costa Rica, San José 11501, Costa Rica.*
[2] *Escuela de Física, Universidad de Costa Rica, San José 11501, Costa Rica.*
*Corresponding author; email: natali.morasandi@ucr.ac.cr

(Received: June 24, 2024; Accepted: November 6, 2024)

RESUMEN

Se analiza la presencia de brisa marina (BM) en nueve estaciones meteorológicas al noroeste de Costa Rica (Península y Golfo de Nicoya, GF); dos del experimento Ticosonde-NAME, Universidad de Costa Rica, y siete del Instituto Meteorológico Nacional, para el 1 de julio al 16 de septiembre de 2004. Se aplica un algoritmo de detección objetiva de BM a datos horarios de las estaciones y temperatura del mar (TM) que utiliza el gradiente de temperatura y la dirección del viento. Las estaciones Pinilla y Guacalillo muestran 64% de BM en los 78 días analizados. Liberia (20 km tierra adentro) presenta un 44.9% de BM asociada a vientos sinópticos débiles del este. Puntarenas presenta casos dudosos por errores en el viento, mientras que las otras estaciones no presentan las series completas. Algunos de los días sin BM son dominados, por un lado, por un fuerte flujo sinóptico del noreste asociado al chorro de bajo nivel del Caribe durante lapsos de reducción de lluvia y, por otro, a flujo sinóptico del suroeste asociado al tránsito de sistemas meteorológicos en el Caribe occidental. El algoritmo muestra buena habilidad para detectar la BM, a pesar de la escasa resolución espacial de la TM. Coherente con una circulación típica de BM, la precipitación en casi todas las estaciones se caracteriza por actividad convectiva costera y precipitación en horas de la tarde-noche. Los resultados son alentadores por su aplicación potencial a actividades de pesca artesanal, agricultura y turismo, así como a la calidad regional del aire, ya que en el GN hay puertos muy activos (Puntarenas y Caldera) y puntos de intenso movimiento de barcos turísticos y comerciales que impactan negativamente las condiciones ambientales.

ABSTRACT

The presence of sea breeze (SB) is analyzed at nine meteorological stations in the northwest of Costa Rica (Peninsula and Gulf of Nicoya, GF); two from the Ticosonde-NAME experiment, University of Costa Rica, and seven from the National Meteorological Institute, for the period from July 1 to September 16, 2004. An objective detection algorithm for SB is applied to hourly data from the stations and sea surface temperature (SST). The algorithm uses temperature gradient and wind direction. Pinilla and Guacalillo stations show 64% of SB on the 78 days analyzed. Liberia (20 km inland) presents 44.9% of SB associated with weak synoptic winds from the east. Puntarenas presents doubtful cases due to wind errors, while the other stations do not present complete records. Some of the non-SB days are dominated, on one hand, by strong synoptic flow from the northeast associated with the low-level Caribbean jet that in turn coincides with the periods of reduced rainfall or mid-summer drought and, on the other hand, by synoptic flow from the southwest associated with the passage of weather systems in the western Caribbean. The algorithm shows a good ability to detect SB despite the poor spatial resolution of SST. Consistent with a typical SB circulation, precipitation at almost all stations is characterized by coastal convective activity and precipitation in the late afternoon and evening hours. The results are encouraging for their potential application to artisanal fishing, agriculture, tourism, and regional air quality, as there are very active ports in the Gulf of Nicoya (Puntarenas and Caldera), points of intense movement of tourist and commercial ships that negatively impact environmental conditions.

Keywords: midsummer drought, Caribbean low-level jet, land/sea breeze, mesoscale/synoptic interactions, Central America.

1. Introduction

Wind circulation has been studied for thousands of years. Estoque (1961, 1962) and Neumann and Mahrer (1971) inspired some of the theoretical foundations of sea breeze (SB), the most common low-level wind circulation at many coastal locations. Afterward, many papers have covered this mesoscale flow, using experimental frameworks (Mitsumoto et al., 1983; Intrieri et al., 1990), numerical modeling (Abbs, 1986; Mora et al., 2020; He et al., 2022; Román-Cascón et al., 2022), and theoretical approaches (Qian et al., 2009; Drobinski et al., 2011). Research combining numerical and observational approaches, such as the studies by Abbs (1986), Mora et al. (2020), Rafiq et. (2020), and Reddy et al. (2022), is very valuable to understanding the physical and dynamical processes of the SB. However, in Central America, these investigations are scarce (Mora et al., 2020). In Costa Rica, Mora et al. (2020) used a numerical-observational approach to examine the structure, the inland penetration, and the precipitation distribution due to the SB front during a special local campaign (Ticosonde-NAME) along the Grande de Tárcoles river basin (GTRB); they found that maximum precipitation occurs between 14:00-17:00 local solar time (LST), showing a time lag of 2-3 h after the temperature maximum, suggesting that local diurnal heating is key to convection. The SB maximum inland incursion was 24 km, with no evidence of its penetration into the Central Valley. July-August precipitation exhibited a rainfall decrease along the GTRB due to the SB dynamical processes interaction with larger-scale systems, such as the Caribbean low-level jet (CLLJ).

The mesoscale SB processes have also been studied in the framework of similar or larger-scale domains using various datasets gathered by different acquisition equipment. For example, Guille et al. (2003, 2005) used QuikSCAT data to analyze the global signals of SB, especially over the oceans. However, their results lacked specific features, such as the complex topography in the region, which is a relevant element in defining local circulations such as the SB. Pérez et al. (2018) characterized the SB phenomenon using station data along the Colombian Caribbean coastline; the study found that the marine breeze signal on the Colombian Caribbean coast is stronger during the dry season (December-March), when it reaches the highest gradients of sea/land temperature and with a predominantly diurnal component.

Allende-Arandía et al. (2020) investigated the diurnal wind component associated with the breeze phenomenon in Sisal, Yucatan, Mexico. Their results indicated that Sisal (inland) experienced a large diurnal cycle of ~5 ºC, and thermal differences of about 4 ºC. In this work, the diurnal signal at most inland stations is in the order of 6-8 ºC, implying less inland penetration of the SB front with wind speeds in the range of 2-4 m s^{-1} and confirming the role of the thermal contrast in developing SB winds. Several recent studies have also considered that the direction and strength of the synoptic-scale flow also affect the structure and evolution of the SB (Azorin-Molina and Cheng, 2009; Anjos and Lopes, 2019; Mora et al., 2020; di Bernardino et al., 2021; Reddy et al., 2021). However, other aspects such as topography (Abbs, 1986; Abel et al., 2007; Qian et al., 2009; Davis et al., 2019), type of surface-sea barrier such as mangroves (Lizano et al., 2001), and shape of coastline (Abbs, 1986) affect the SB circulation, mechanism driven by the differential heating between the land and sea surfaces.

Due to the relevance of the direct effect of SB on weather patterns of temperature, precipitation, wind speed, and direction in coastal regions and adjacent inland areas, it is important to continue improving our understanding of this local circulation, its impact, and potential benefits to tourism and fishing operations, two of the most important activity for local development, as generators of employment in coastal areas. The present study is an extension of Mora et al. (2020), who analyzed the structure and evolution of the SB along the GTRB in Costa Rica from July to September 2004. In this research, the emphasis is given to the characterization of SB circulations in the Peninsula of Nicoya (PN) and the Gulf of Nicoya (GN) in northwestern Costa Rica for the same period studied in Mora et al. (2020). The PN is of huge importance for the country's economy, as artisanal fishing, agriculture, and tourism are the most significant socio-economic activities. In addition, the second busiest airport in Costa Rica, Liberia's Daniel Oduber International Airport, is located in the northern part of the peninsula. The PN is also one of the world's seven Blue Zones, geographical areas with

a high concentration of long-lived populations based on a healthy and outdoor lifestyle (Madrigal-Leer et al., 2020).

Using station and gridded data, the objective of this work is to analyze the coastal evolution of the SB in the GN and its relationship with the intensity of the CLLJ. Mora et al. (2020) results will be contrasted with the ones obtained here to validate their findings for a larger domain, the PN. To better delineate the scope of this work, the paper has been organized as follows. The study area is presented in the next section. Data information, quality control, and analytical and statistical procedures are discussed in section 3, which also describes the SB detection algorithm and the definition of indexes for the CLLJ and the MSD, two systems of a scale larger than that of the SB, to explore some of their interactions. In section 4, the results are discussed. Section 5 finally summarizes the conclusions of this study.

2. Study area

The PN is on the northwestern Pacific coast of Costa Rica (Central America), being the largest peninsula in the country. It comprises regions of Guanacaste and Puntarenas provinces and has an area of ~5157 km^2 (personal communication), about 2.1% of the Costa Rican territory. The PN is limited to the east by the Tempisque River and the GN, to the north by the Gulf of Papagayo, and to the south and west it is bounded by the Pacific Ocean (Fig. 1). The PN is a relatively flat terrain with a well-defined dry season

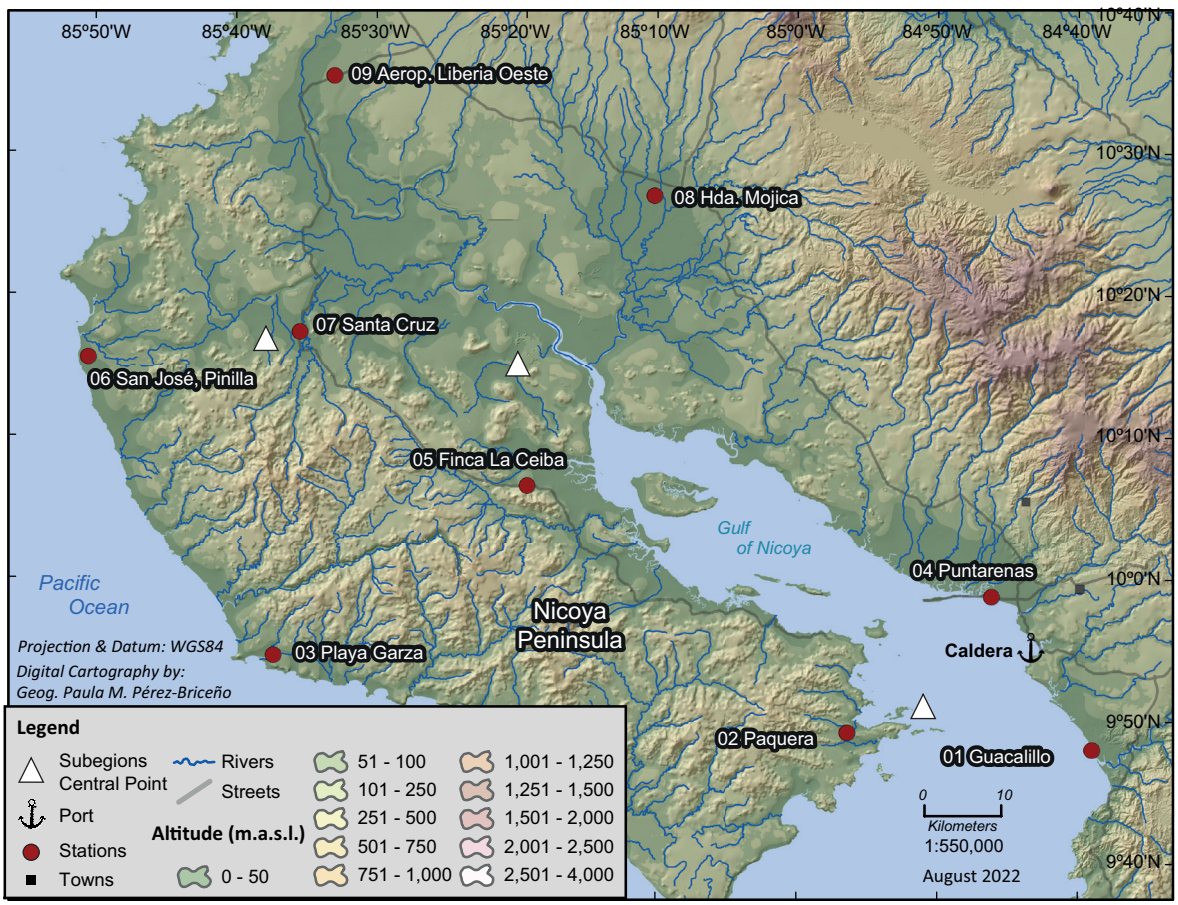

Fig. 1. Location of the nine meteorological stations distributed over the Peninsula of Nicoya (PN) and nearby regions. The triangle marker represents the subregions' central points: (a) Gulf of Nicoya, (b) western PN, and (c) central PN (see Table I for details).

from December to April and a wet season from May to November (Whelan, 1989), with a relative minimum of precipitation during July-August, known as the midsummer drought (MSD, Magaña et al., 1999). This decrease in rainfall marks a bimodal precipitation annual cycle over the Central America Pacific slope, with two maxima in June and September-October (Magaña et al., 1999; Maldonado et al., 2016).

The GN is a tectonic estuary east of the peninsula, consisting of a shallow body of water between the peninsula and Costa Rica's mainland. Rivers such as the Tempisque, Tárcoles, and Barranca carry freshwater into the Gulf of Nicoya. The estuary is one of the most important fishing grounds of Costa Rica and one of the world's most productive tropical estuaries (Alms and Wolff, 2019). A large part of the coastal residents in GN depend on artisanal fishing for their living. Unfortunately, the intense use of natural resources, excessive urbanization, and industrial and agricultural pollution have negatively impacted their inhabitants (Castro-Campos and Jiménez-Ramón, 2021). Also, this region includes the two major Costa Rican ports along the Pacific coast, Puerto Caldera and Puntarenas, both being relevant points for touristic cruises and industrial ships and hosting multiple businesses.

3. Data and methods

3.1 Station data

To analyze the SB diurnal cycle and its relationship with other meteorological variables and atmospheric processes, surface data from nine automatic stations were used. Hourly data from seven stations located on the PN and surroundings were provided by Costa Rica's National Meteorological Institute (IMN, by its Spanish acronym) for the period July 1 to September 16, 2004 (78 days). Hourly records from the other two stations were obtained through the Ticosonde-North American Monsoon Experiment (Ticosonde-NAME) and a local campaign by the University of Costa Rica and the National Meteorological Institute to complement the analysis. The spatial distribution of all nine observing sites is shown in Figure 1.

To characterize the representative patterns of the observed diurnal cycle of precipitation and temperature, the time series of the 1-h accumulated precipitation and mean temperature were computed for all the stations in LST. Temperature and surface wind records were used to develop a simple algorithm to detect SB. The information about the automatic meteorological stations is shown in Tables I and II. Note from Fig. 1, that Puerto Caldera lies between Puntarenas and Guacalillo, stations examined in this study.

3.2 Gridded data

Since one of the primary drivers of the SB circulation is the difference between air temperature over land and sea surface temperature (SST), SST data were necessary to identify SB days. Global daily SST estimates were derived from measurements carried out by the infrared sensors onboard polar-orbiting satellites: the Advanced Very High-Resolution Radiometers (AVHRRs), the Along Track Scanning Radiometers (ATSRs), and the Sea and Land Surface

Table I. List of stations with the corresponding central points of regions S1, S2, and S3.

Station number	Station name	Latitude (N)	Longitude (W)	Altitude (masl)	Central point
1	Guacalillo	09º 48' 0.5"	84º 38' 52"	24	S1: [09º 54' 37.5", 84º 50' 37.5"]
2	Paquera	09º 49' 17"	84º 56' 20"	10	
3	Puntarenas	09º 58' 49"	84º 46' 12"	3	
4	Finca La Ceiba	10º 06' 40"	85º 19' 03"	58	S2: [10º 15' 0", 85º 19' 30"]
5	Santa Cruz	10º 17' 07"	85º 35' 30"	40	
6	Hacienda Mojica	10º 27' 10"	85º 09' 55"	33	
7	Playa Garza	09º 54' 49"	85º 36' 55"	10	S3: [10º 16' 15.6", 85º 37' 30"]
8	Pinilla	10º 15' 36"	85º 50' 16"	15	
9	Aeropuerto Liberia	10º 35' 20"	85º 33' 08"	89	

Table II. Percentage (%) of missing data per meteorological variable and by gauge station.

Station number	Station name	Temperature	Precipitation	Wind	Operated by
1	Guacalillo	17.7	17.7	17.7	Ticosonde-NAME
2	Paquera	0	0	100	IMN
3	Puntarenas	21.2	21.3	21.3	Ticosonde-NAME
4	Finca La Ceiba	37.6	37.6	37.6	IMN
5	Santa Cruz	0	0	46.7	IMN
6	Hda. Mojica	0	0	11.5	IMN
7	Playa Garza	0	0	83	IMN
8	Pinilla	0	0	0.05	IMN
9	Aeropuerto Liberia	0.5	0.5	0.5	IMN

INM: National Meteorological Institute.

Temperature Radiometer (SLSTR). These data are provided at different processing levels, in this study, the product Level 4 (L4) containing daily data at 0.05º × 0.05º horizontal grid resolution was used. Merchant et al. (2019) provide a complete description of this SST dataset. According to the authors, the evaluated global median uncertainty for the SST pixel is 0.18 K.

Hourly zonal wind at 10 m (u10) from ERA5 reanalysis (Hersbach et al., 2020) and daily incoming radiation data from CLARA-A2 (Karlsson et al., 2017) were used to explore the potential interaction between the CLLJ and the MSD with the SB circulation, respectively (details in sections 3.4 and 3.5). Both datasets provide information on a rectangular grid of 0.25 × 0.25º. Surface incoming shortwave (SIS) radiation from CLARA-A2 consists of cloud, surface albedo, and surface radiation budget products also derived from the AVHRR sensor carried by polar-orbiting, operational meteorological satellites. Uncertainties are associated with cloud masking.

3.3 The sea breeze detection algorithm

Azorin-Molina et al. (2011) developed a method for identifying SB days (SBd) using 30-min surface observations of wind, temperature, relative humidity, and precipitation. Their algorithm requires three conditions (named filters 1 to 3) for SB detection and another three for confirmation. Filter 1 requires the 30-min wind speed mean and maximum curves to steadily increase from sunrise until midday and gradually decrease afterward until sunset. In filter 2, the 30-min wind direction must show onshore flow after sunrise. Filter 3 is the detection of onshore flow for at least 2 h.

Using 3-hourly surface data and 6-hourly radiosonde measurements, Masouleh et al. (2019) identified SB when the following conditions were met: (1) days with positive temperature difference between land and sea surface; (2) offshore wind speed at 700 hPa less than 7.5 m s^{-1}, between 12:00 and 14:00 LST; (3) either of these two situations occur: (a) calm condition or offshore wind in the early morning with onshore flow in the afternoon, followed by calm or offshore wind in the night, or (b) afternoon wind speeds greater than 1.5 m s^{-1} on days with light onshore breeze (less than 2 m s^{-1}) during the morning and evening hours, and (4) afternoon SB detected in at least two consecutive readings (at least 3 h).

Based on the above criteria and given the data availability on the region of study (Table II) and the temporal resolution of wind and temperature measurements, an algorithm is proposed here to determine SBd. The following three criteria are necessary for SB occurrence. (1) Days with maximum temperature over land greater than the surrounding SST. The daily SST value used here results from averaging nine grid points located near each station's coast. (2) Offshore wind for at least 3 h between 00:00 and 06:00 LST. (3) Onshore wind for at least 3 h between 12:00 and 18:00 LST. This algorithm was applied to data collected at the stations in Guacalillo, Puntarenas, Pinilla, and Aeropuerto Liberia, whose coastlines are oriented from southeast to northwest, east to west, south to north, and southwest to northeast, respectively.

The former three are coastal stations, while the latter station is located further inland and provides information on the extent of the intrusion of the SB in a relatively flat terrain.

The SB detection algorithm was performed using a Python computing environment (van Rossum and Drake, 2009). It does not include filters to confirm an SB event, as in Azorin-Molina et al. (2011), which can lead to some false positives. Data formatting and plots were prepared using the collection of Python packages.

3.4 Caribbean Low-Level Jet Index

The interaction between the CLLJ and the SB over the Peninsula and the Gulf of Nicoya was analyzed using the Caribbean Low-Level Index (CLLJI) based on the index proposed by Muñoz et al. (2008) and defined as an area average of u10 daily values over the CLLJ region (12º-16º N, 70º-80º W). Long-term seasonal averages (July-September) of hourly u10 over the CLLJ region were calculated for the period 1981-2020. The Strong CLLJI case (SC) was defined in terms of daily values of u10 under the 33rd percentile (–15.7 m s^{-1}) of the seasonal values during the period of study. A Weak CLLJI case (WC) was identified when daily values of u10 surpassed the 66th percentile (–13 m s^{-1}) of the seasonal values. For each of the SBd identified at the gauge stations, the CLLJ intensity was determined and used to explore its effect on the SB characteristics. As a result, the SBd are categorized into three groups under the influence of: (1) SB and SC (SB + SC); (2) SB and WC (SB + WC), and (3) SB and normal CLLJI.

3.5. The midsummer drought identification

To improve prediction in the tropics, an important problem to be tackled first is the lack of dynamic knowledge about the atmospheric transition mechanisms between different precipitation modes. The SB circulation is one the main rain producing systems, especially in the tropics, characterized by its variability in time (intra to seasonal scales) and landforms (curved or linear coasts, for instance). Gouirand et al. (2020) addressed the problem of the interannual variability of changes between summer-winter and winter-summer in the Caribbean and Central America. According to these authors, the above two changes reveal asymmetries in the annual cycle; however, in their research, no dynamic mechanisms were discussed. On seasonal time scales, MSD is perhaps the most difficult tropical feature to account for.

In this research, the approach to characterizing that feature is made through the inclusion of different parameters to identify the MSD, and to put forward a simple dynamical approach using precipitation, SIS, and maximum and minimum air temperatures (Tmax and Tmin, respectively), following a conceptual model proposed by Amador and Arce-Fernández (2022). The model is partially based on the schematic diagram of the dynamics of the MSD by Magaña et al. (1999), where the offshore extension of the MSD was not estimated due to a lack of marine data; however, in Amador and Arce-Fernández (2022), the use of lightning data from the World Wide Lightning Location (WWLLN) network allowed to estimate ~500 km of it in the Gulf of Papagayo. Besides, the former work introduced a basic idea of the interaction of diurnal radiation changes, the cloud response, and the inland temperature reaction during MSD events. The conceptual model proposed by Amador and Arce-Fernández (2022) is described below.

MSD is a reduction of precipitation between two Pacific regional maxima in June and September-October. With fewer pentad convective clouds during the MSD on average, a major amount of SIS should reach the ground during that pentad, so the Tmax should increase during that MSD subperiod. Since almost cloudless nights may be expected with fewer daylight convection, Tmin must decrease due to an increased amount of surface outgoing infrared radiation. To test this simple dynamical model, the daily data (78 days) for all variables mentioned above for the three regions described in section 2.3 were grouped in 5-day periods (pentad values); after that, the anomalies are estimated as the difference between each pentad and the mean pentad value for the period of study.

To identify and characterize the MSD, time series of maximum and minimum temperature, precipitation, and radiation were obtained for three subregions (S), each of them defined as a 3-station group: Gulf of Nicoya (S1; Guacalillo, Paquera, and Puntarenas), Central PN (S2; La Ceiba, Santa Cruz, and Hacienda Mojica), and Western PN (S3; Playa Garza, Pinilla, and Liberia). The incoming shortwave radiation time series for S1, S2, and S3 were calculated, respectively,

from averages of the 8, 10, and 12 grid points enclosing their 3-station groups and then normalized to account for different area sizes due to the asymmetric distribution of the grid points in each subregion. The central points of the defined subregions are marked with a white triangle in Figure 1.

At this point, it is important to question the relationship between the MSD active period and the development of the Pacific land and SB. A crucial problem arising from the above synoptic-mesoscale interaction is to what extent the intensity of the CLLJ winds inhibits the evolution of the sea/land breezes and the conversion processes amidst them. The CLLJ also plays a relevant role in the convergence of moisture flux in the nearby region of Colombia, a mechanism that may inhibit or not convection associated with the SB processes (Hoyos et al., 2018). As suggested by Reddy et al. (2023), other variables, such as the lower atmosphere vertical wind shear, are crucial for the start of convection and thunderstorm activity.

4. Results

4.1 Diurnal cycle

Figure 2 shows the diurnal variations of surface air temperature (solid red line) and rainfall (blue bars) in the nine meteorological stations analyzed. Tmin is reached between 05:00 and 06:00 LST for all stations, and Tmax (approx. 31 ºC) near 12:00 LST in the three coastal areas, Guacalillo, Playa Garza, and Pinilla (Fig. 2a, g, h) and 1 h later at the inland stations, La Ceiba, Santa Cruz, Hacienda Mojica, and Liberia (Fig. 2d-f, i). After the midday peak, the temperature decreased through the afternoon and continued to cool slowly down overnight. This suggests that solar heating plays an important role in

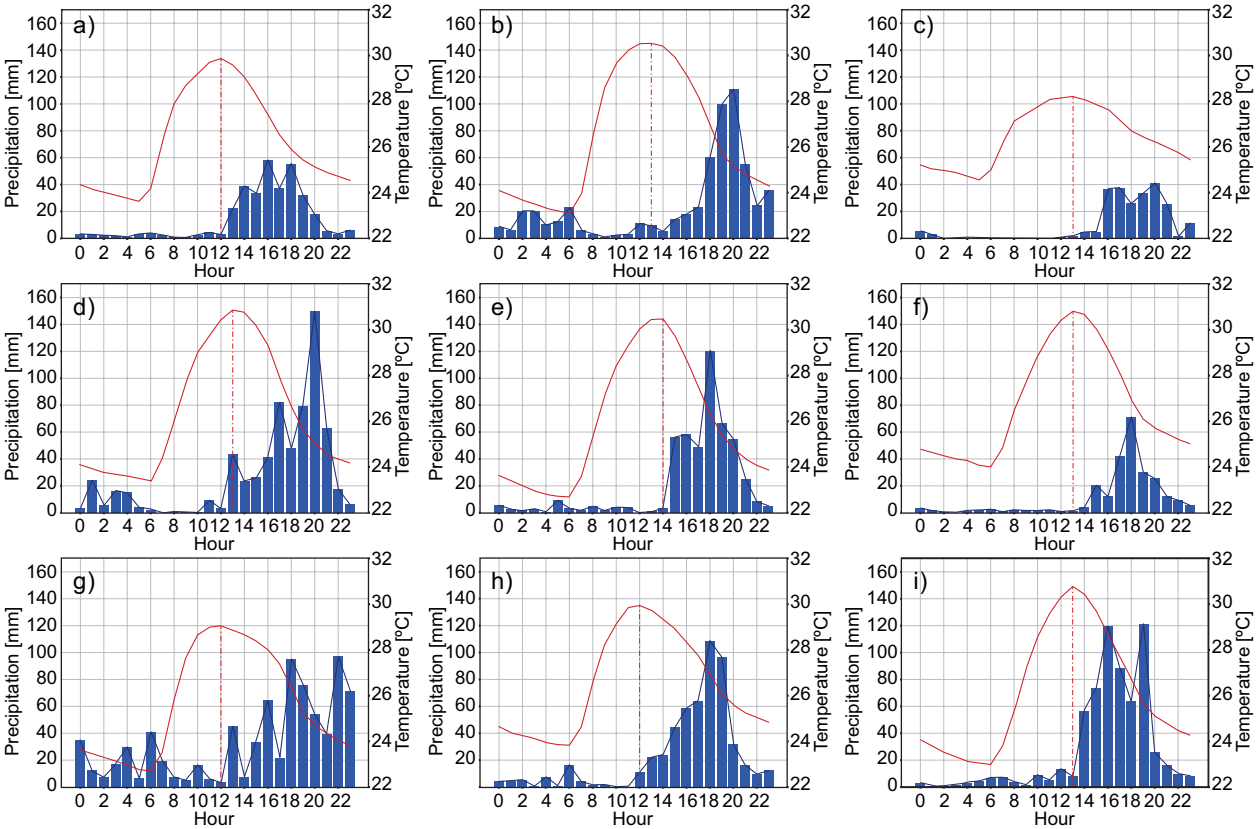

Fig. 2. Right axis: hourly mean temperature (ºC, solid red line; the red vertical dashed line represents the hour of maximum temperature). Left axis: hourly total precipitation (mm) distribution. For (a) Guacalillo, (b) Paquera, (c) Puntarenas, (d) La Ceiba, (e) Santa Cruz, (f) Hacienda Mojica, (g) Playa Garza, (h) Pinilla, and (i) Liberia.

temperature variability. Higher precipitation occurs in the afternoon-night period (between 14:00 and 21:00 LST), showing a lag of 4-6 h after the Tmax peak. These results are consistent with the spatial-temporal distribution of precipitation observed on the Pacific coast (Ramírez, 1983; Curtis, 2004; Mora et al., 2020; Wiggins et al., 2023).

In almost all stations, an accumulation of precipitation is observed during the early morning hours, especially in the coastal stations of Paquera and Playa Garza (Fig. 2b, g), followed by La Ceiba and Pinilla (Fig. 2d-h). The observed morning precipitation could be associated with convective activity, consistent with the average oceanic monthly maximum lightning density in this region for July, August, and September (Amador and Arce-Fernández, 2022). The SB circulations play an important role in the climate and atmospheric environment of coastal and adjacent inland areas, having a direct effect on weather patterns of temperature, precipitation, and wind. Therefore, describing the diurnal variations of these variables is essential for understanding the local climate and the SB dynamics and their interaction with the weather patterns.

4.2 Wind and precipitation

Figure 3 shows the distributions of 2-m wind speed and direction during the detected SBd. In all four stations, weak offshore wind occurs during the early morning hours (00:00-06:00 LST). In this time slot, wind intensities range between 2 and 4 m s^{-1} in Pinilla and Liberia, while in Puntarenas and Guacalillo the magnitudes do not exceed 2 m s^{-1}. The morning time (06:00-12:00 LST) can be regarded as a transition period, in which onshore winds begin to predominate due to land surface heating. Note that, in this case, wind magnitudes increase, with most of the values ranging from 2 to 6 m s^{-1}. In the afternoon (12:00-18:00 LST), relatively stronger onshore winds (with magnitudes greater than 4 m s^{-1}) prevail, indicating the occurrence of SBd. Lastly, offshore winds (with weak intensities) return during the night (18:00-00:00 LST) due to nearby land surface cooling, and probably the presence of katabatic winds related to the mountain range to the east. Studies such as Mapes et al. (2003a, b) have shown that the mean local diurnal cycle over tropical regions can be affected by several factors, including topography.

Using in situ observations, Davis et al. (2019) found a cross-shore wind speed of more than 8 m s^{-1}, while WRF-modeled data presented larger amplitudes of the sea/land breeze with altitude from the coast over the Red Sea and the coastal Arabian Peninsula. A similar result was exhibited by the SB in Mora et al. (2020, see Fig. 3), where two of the in situ stations used (Lagunilla [9.85-84.61º, 172 m] and Orotina [9.94-84.54º, 185 m]) presented cross-shore westerly maximum winds of 4 to 5 m s^{-1}. Those observations were taken along a station profile from the Gulf of Nicoya to the steeper lands to the east. Results here are also in good agreement with the work of Allende-Arandía et al. (2020) in Sisal, Yucatan, Mexico, and Ma et al. (2021) for the Yellow Sea, China. The diurnal signal at most inland stations analyzed by Allende-Arandia et al. (2020) was in the order of 6-8 ºC, implying less inland penetration of the SB front with wind speeds in the range of 2-4 m s^{-1}. Ma et al. (2021) reported that "the biggest average horizontal SB wind speed was 5.6 m s^{-1} at 425 m, and 4.5 m s^{-1} at 375 m".

Two types of non-SBd were identified. The first type, shown in Figure 4, corresponds to days in which strong northeasterly synoptic flow dominated over the region of study (hereafter referred to as NEd), associated with the MSD and enhanced CLLJ conditions. In addition, Liberia is under the influence of strong easterly gap winds; therefore, the number of NEd is greater in this station (48.7% of the total days). On the other hand, the second type (Fig. 5) involved days with predominant southwesterly synoptic forcing and maximum temperature over land equal to or less than SST (hereafter referred to as SWd) due to the presence of, for example, tropical disturbances in the Caribbean Sea, such as hurricane Ivan on September 2-24 (IMN-MINAE, 2004), or the transit of tropical waves. In Pinilla, Guacalillo, and Liberia, 5 SWd were detected, corresponding to less than 8% of the total days, while 26 were found in Puntarenas (42.6% of the available days). The urban character of the station in Puntarenas and its location on a narrow strip of land may explain the large difference in SWd compared to Guacalillo.

According to the detection algorithm, Pinilla, Guacalillo, Liberia, and Puntarenas presented 53, 41, 35, and 17 SBd, respectively, within the period of study (see Table III). The second and last stations

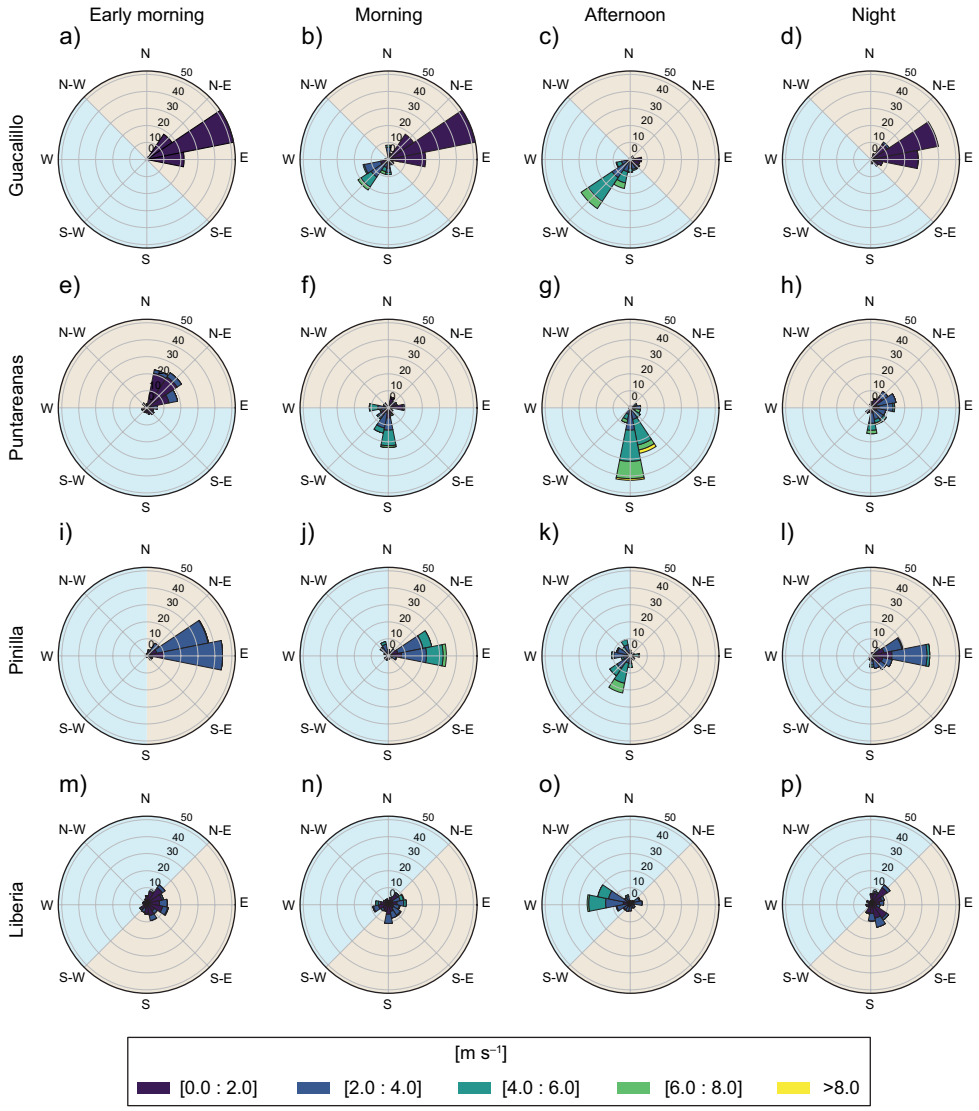

Fig. 3. Distribution of 2-m wind speed (m s^{-1}) and direction in the early morning, morning, afternoon, and night during detected SBd for (a-d) Guacalillo, (e-f) Puntarenas, (i-l) Pinilla, and (m-p) Liberia. The light blue (light brown) sector is the direction of onshore (offshore) winds. See text for definitions.

have a greater percentage of missing data (17.7% in Guacalillo and 21.3% in Puntarenas), which could have masked the number of SBd. Besides, wind data in Puntarenas requires further revision. In Pinilla and Guacalillo, SBd occurs in more than 64% of the total days (Totald). The station in Liberia, which is located approximately 20 km inland, registers nearly half (44.9%) of the available days under SB conditions. This penetration of the SB occurs during periods with weaker easterly winds and is facilitated by the relative flatness of the terrain. Regarding inland penetration, in some regions terrain shape and vegetation may inhibit large-distance incursions from the coast, although there are cases where studies have reported that the SB front entered 170 km in Bohai Bay, China (Li et al., 2023) and that it was still evident 280 km inland in the Gulf of Carpentaria in northern Australia (Physick and Smith, 1985).

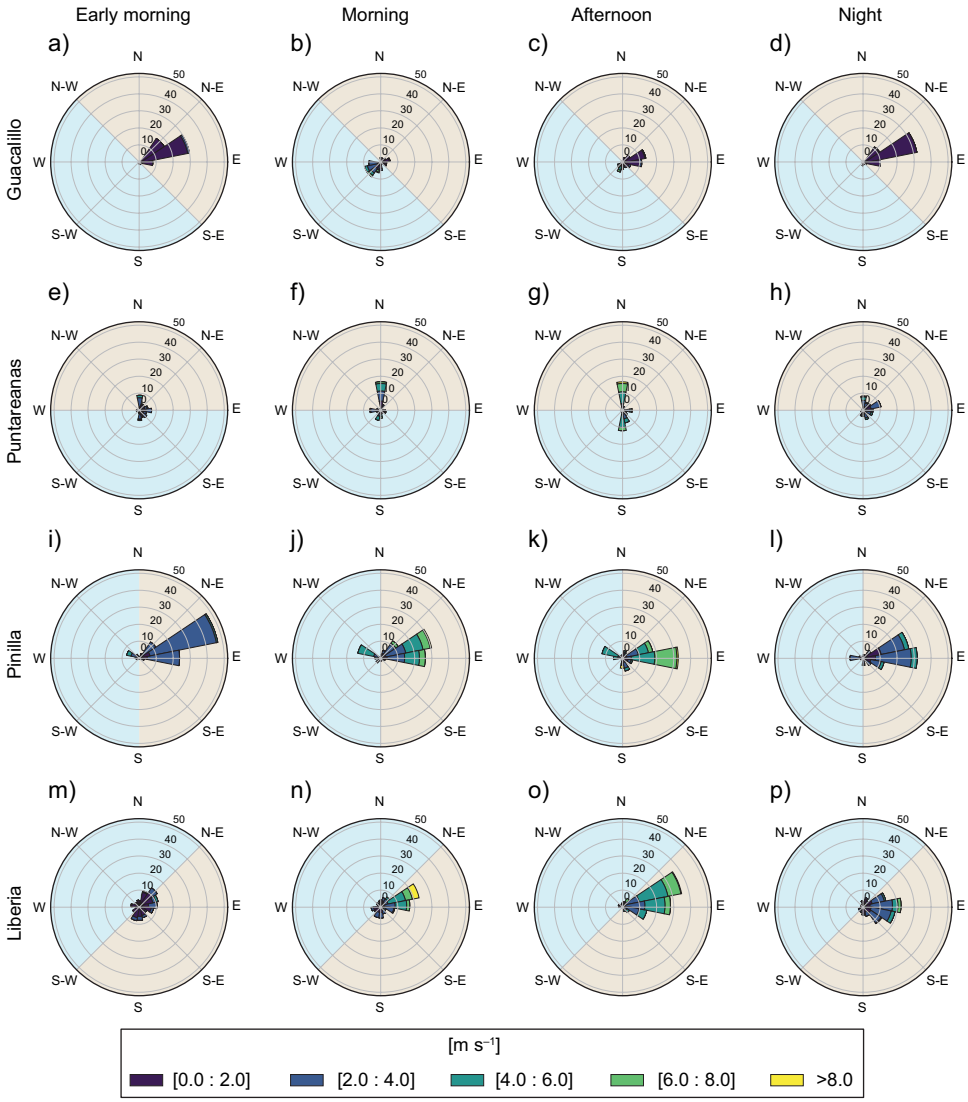

Fig. 4. Distribution of 2-m wind speed (m s^{-1}) and direction in the early morning, morning, afternoon, and night during detected NEd for (a-d) Guacalillo, (e-f) Puntarenas, (i-l) Pinilla, and (m-p) Liberia. The light blue (light brown) sector is the direction of onshore (offshore) winds. See text for definitions.

To determine the relation between the CLLJ and the occurrence of NEd events, the CLLJ area proposed by Amador (2008) is used to identify days under the influence of strong synoptic flows associated with intense Low-Level Jet conditions. These days are characterized by wind magnitudes over the CLLJ area greater than or equal to its 78-day average plus one standard deviation. In Table III, the values in bold parentheses indicate the number of strong CLLJ days associated with NEd, corresponding to 16% to 23% of the detected events.

The mean diurnal cycle of precipitation and temperature during SBd and non-SBd is shown in Figure 6. In Guacalillo, Pinilla, and Liberia, precipitation mainly occurs in the afternoon during SBd, in response to land surface heating and the associated triggering of convective activity. In Puntarenas, the SWd contributes to most of the accumulated rainfall,

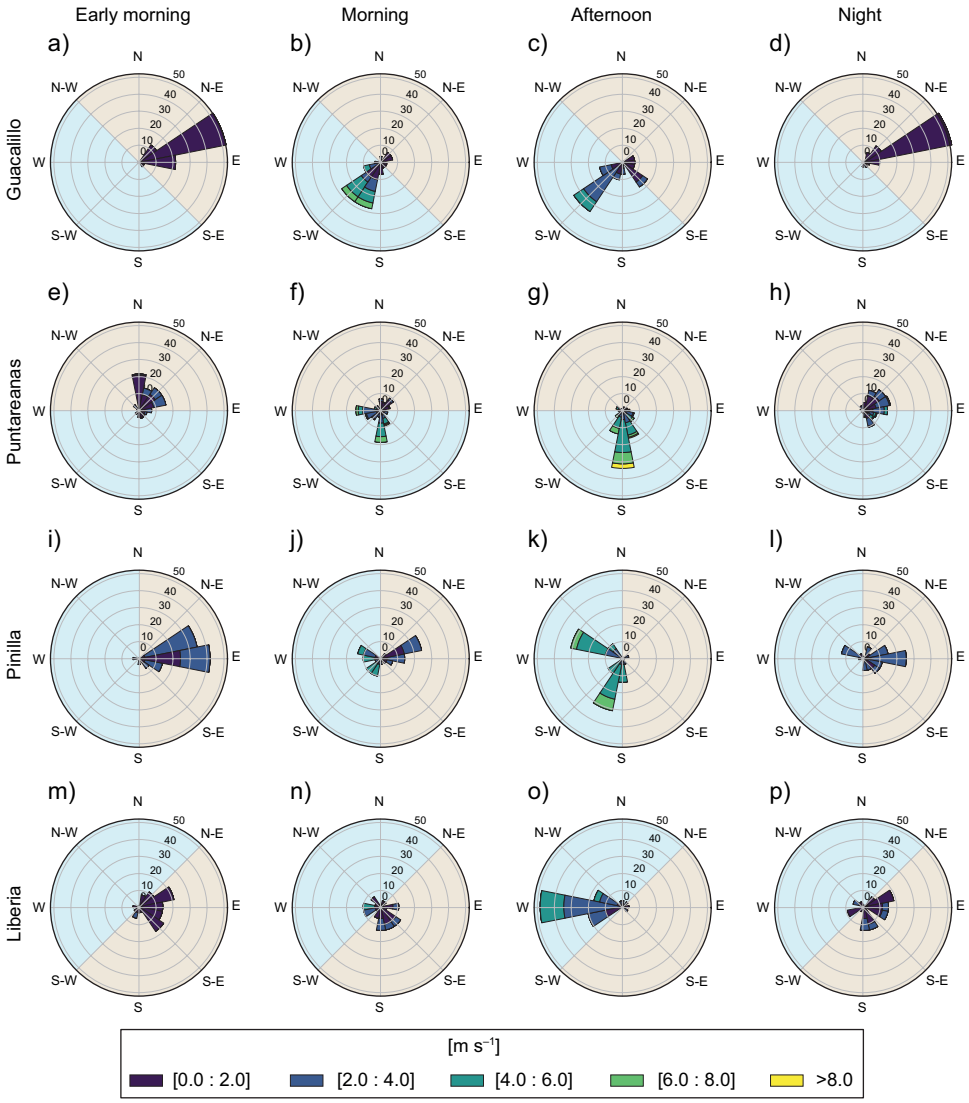

Fig. 5. Distribution of 2-m wind speed (m s^{-1}) and direction in the early morning, morning, afternoon, and night during detected SWd for (a-d) Guacalillo, (e-f) Puntarenas, (i-l) Pinilla, and (m-p) Liberia. The light blue (light brown) sector is the direction of onshore (offshore) winds. See text for definitions.

Table III. Absolute and percentage counts of SBd, NEd and SWd, compared to the Totald. Values in bold indicate the number of strong CLLJ days associated with NEd events (see text for definitions).

Station	Totald	SBd	NEd	SWd
Pinilla	78 (100%)	53 (68.0%)	20 **(4)** (25.6%)	5 (6.4%)
Puntarenas	61 (100%)	17 (27.9%)	18 **(3)** (29.5%)	26 (42.6%)
Guacalillo	64 (100%)	41 (64.1%)	18 **(4)** (28.1%)	5 (7.8%)
Liberia	78 (100%)	35 (44.9%)	38 **(9)** (48.7%)	5 (6.4%)

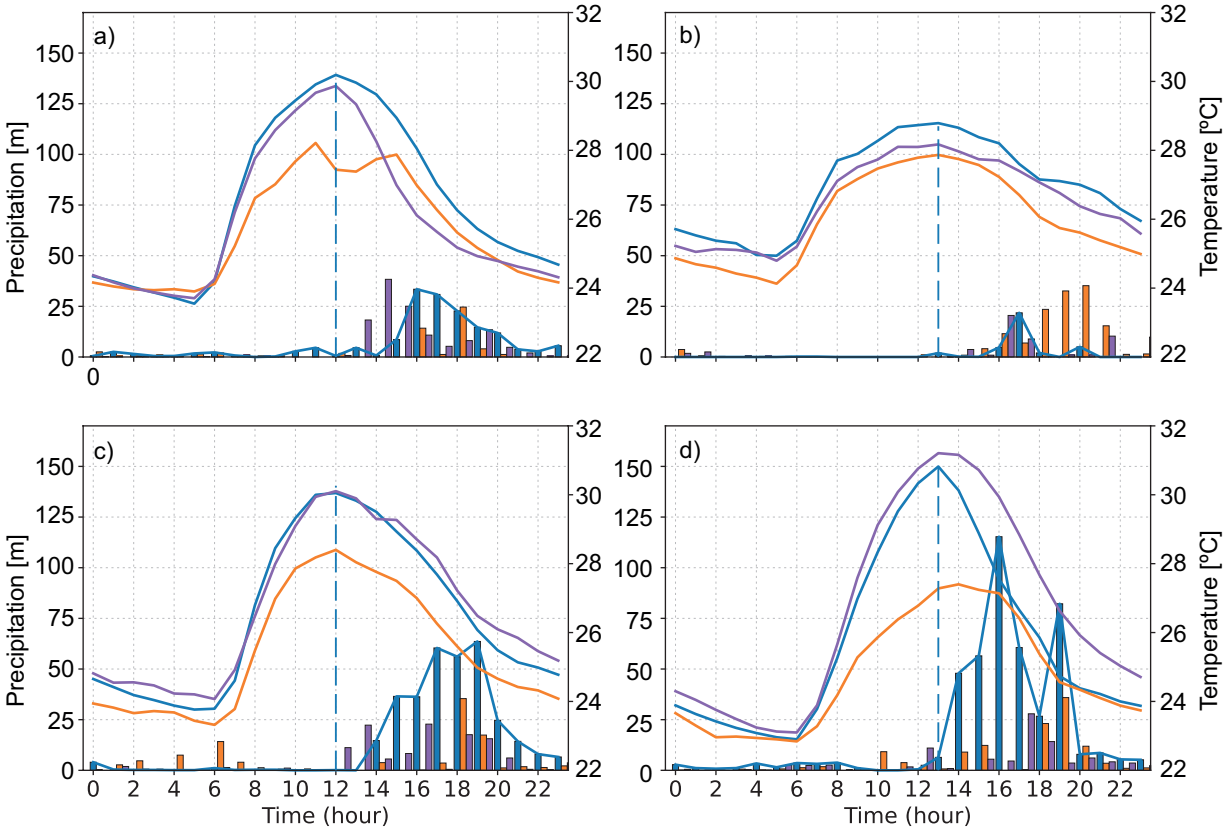

Fig. 6. Mean diurnal cycle of precipitation (bars) and temperature (solid lines) during SBd (blue), NEd (purple), and SWd (orange) days for (a) Guacalillo, (b) Puntarenas, (c) Pinilla, and (d) Liberia. The blue vertical dashed line in each panel shows the time when the maximum temperature is reached during SBd. The blue thin line is the cubic spline interpolation from the blue bars.

followed by SBd. Despite the relative proximity of Guacalillo to Puntarenas, local conditions differ between them; on the one hand, Guacalillo is a site more open to the sea, while Puntarenas is a small coastal city located along a narrow strip of land, as mentioned before.

It is noteworthy that temperatures on SBd are higher than in the rest of the days in Puntarenas and Guacalillo. In Pinilla, the mean diurnal cycles of temperature during SBd and NEd are very similar. However, the strong northeasterly flow in the latter case prevents the development of SB circulations. On SWd, there are much lower land temperatures between 06:00 and 18:00 LST than on other days. This condition does not favor the onset of SBd, because the difference between maximum temperature over land and SST is not positive, which could be related to the occurrence of "temporales" (extended rainfall periods, Amador et al., 2018) and increased cloud cover. The cubic spline curves were drawn to roughly estimate and better visualize the time in which the maximum precipitation occurs at each station after Tmax is registered. The stations show, in general, that the precipitation lags 4-6 h after Tmax, even in the case of Liberia, located over relatively plain terrain.

4.3 Relationship between the sea breeze and the CLLJ

To explore the relation between the SB and the CLLJ, the SBd for Liberia, Guacalillo, and Pinilla are categorized in terms of the daily intensity of the CLLJ. Figure 7 displays the wind rose depicting different periods of the day for the defined SB categories (SB + SC, SB + WC, and SB + normal CLLJI). It is important to note that the CLLJ intensity has a well-defined diurnal cycle, characterized by a minimum during the

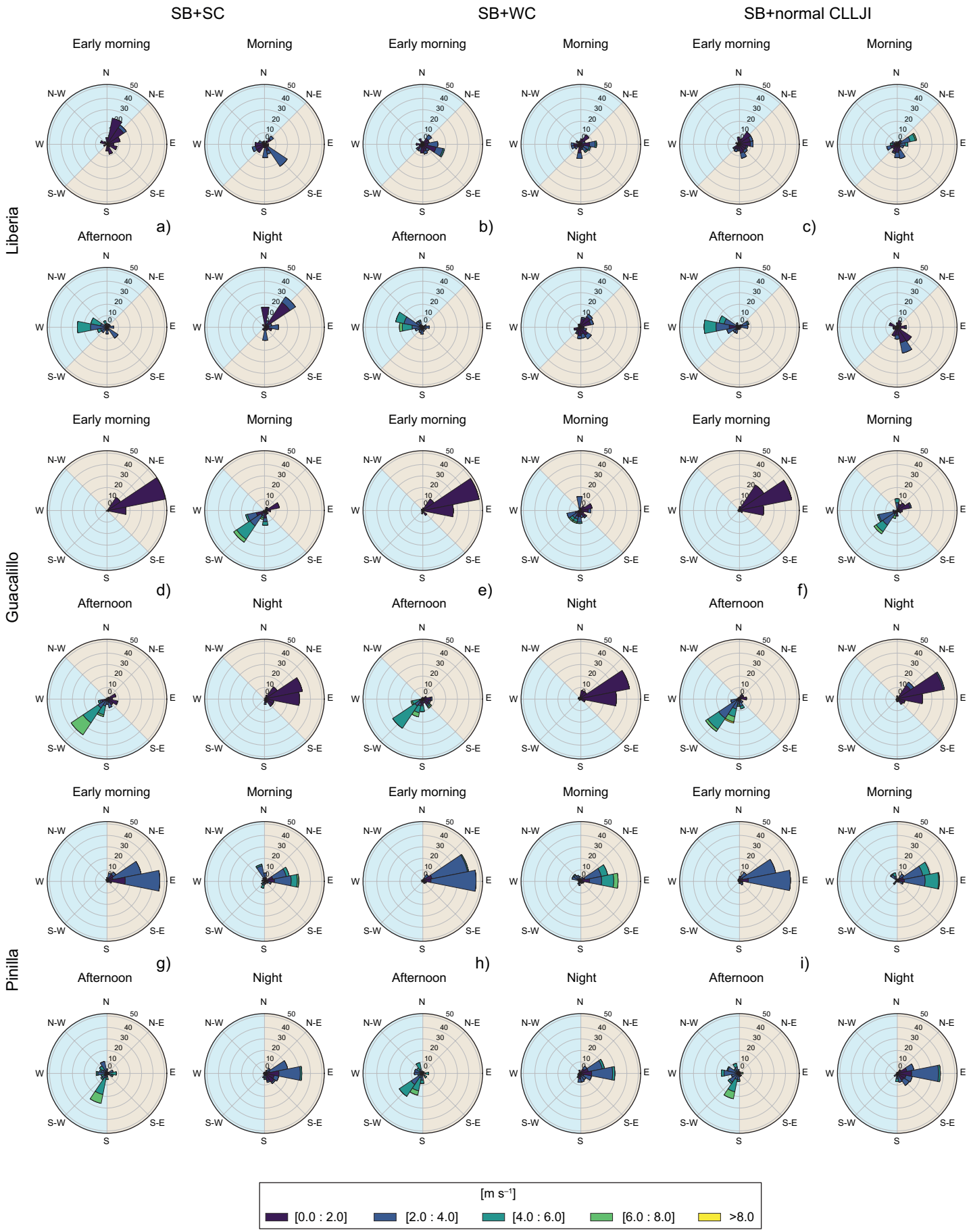

Fig. 7. Wind rose of each category of the sea breeze according to the CLLJ intensity. The top row shows the panels for Liberia, the middle row for Guacalillo, and the bottom row for Pinilla. Panels (a, d, and g) show the cases for SB + SC; (b, e, and h) for SB + WC; and (c, f, and i) for SB + normal CLLJI. The light blue (light brown) sector is the direction of onshore (offshore) winds. See text for definitions.

morning and afternoon and a maximum in the night hours (Cook and Vizy, 2010). This contrast could facilitate the presence of westerly winds associated with the surface temperature-gradient-driven SB in all the studied stations during the hours of lower jet intensity.

In Liberia, during SB + SC (Fig. 7a), northeasterly winds dominate through the night until the early morning, and the SB is established during the afternoon. In addition, there is a southeasterly flow in the morning. On SB + WC (Fig. 7b), the wind intensities during the night, early morning, and morning are weaker than in SB + SC, and the wind directions are more scattered. Thus, the interactions with the synoptic flow are not clear during those periods. The intensity of the SB during the afternoon hours does not seem to be different between SB + SC and SB + WC. In the SB and normal CLLJI category, there is evidence of synoptic wind flow from north and southeasterly trades during the morning and night hours.

All the cases studied in Guacalillo (Fig. 7d-f) indicate that there is no clear influence of SC or WC on the intensity and onset of SB. The nighttime and early morning wind intensity is below 2 m s^{-1}, and its northeasterly direction could be related to local circulations and katabatic winds due to the presence of a mountain range to the northeast of the gauge station. In the afternoon, the southwesterly wind is found in SBd either with SC, WC, or normal CLLJI; therefore, the influence of anabatic winds could be the most important mechanism to reinforce the onshore breeze. The largest difference in the wind flow pattern is found during the morning hours, where the southwesterly flows in both SB + SC and normal CLLJI are stronger than in SB + WC.

Pinilla (Fig 7g-i), does not show a clear difference in the wind circulation during the diurnal cycle. Onshore SB is clearly present during the afternoon. Meanwhile, the easterly wind is dominant during the rest of the day and could interact with the land breeze, mainly during the night and early morning.

The above results indicate that the CLLJ does not clearly modulate the onset and intensity of the registered SB events because it is weak (approximately –12 m s^{-1}) during the daytime hours, while local effects seem to play a more relevant role. Nonetheless, if the CLLJ is sufficiently strong in the morning and afternoon, it can overcome the sea/land flow, as in 16% to 23% of the NEd events).

On the other hand, note that the southwesterly flow registered in most of the stations in the afternoon-evening period can be reinforced by synoptic-scale forcing in the eastern tropical Pacific (Zárate-Hernández, 1977; Amador et al., 2016).

4.4 Midsummer drought

The three subregions (Fig. 8) show a coherent pentad precipitation pattern suggesting the dominance of a mesoscale to synoptic scale system in the region, although some differences among regions a, b, and c are observed. At the beginning of the analysis period, negative precipitation anomalies dominate, followed by a short time of above-normal values. Pentads 7 to 11 (July 31 to August 24) have negative anomalies, mainly, while the rest of the period presents the largest positive anomalies of the whole period. Incoming solar radiation at the surface follows closely, with an apparent lag of one pentad, the precipitation pattern over land regions (b and c), with less radiation flux during rainy pentads (see pentads 1-5, July 1-25) compared with the less rainy five-day periods (see pentads 7-15; July 31 to September 13). Maximum surface temperature also responds closely to the correspondence of positive Tmax anomalies to higher radiation flux and negative precipitation deviations. Tmin has a more complex distribution, although some pentads show a good correspondence between the above relationship and Tmin negative variations. During MSD days, the reduction of precipitation along the Pacific coast suggests stronger than normal sea/land temperature gradients due to an increase in SIS.

A moderate to strong CLLJI is usually associated with a stronger than normal low-level wind shear inhibiting convection and the observed reduction in precipitations in the Pacific lowlands (a basic characteristic of the MSD). During this reduction in precipitation, SB processes continue to work if thermal sea/land gradients allow for it. A more intense CLLJ may imply the reduction of SST near coastlines due to wind stress over the ocean surface, providing favorable conditions for a land-sea breeze to develop depending on the strength of the thermal contrast.

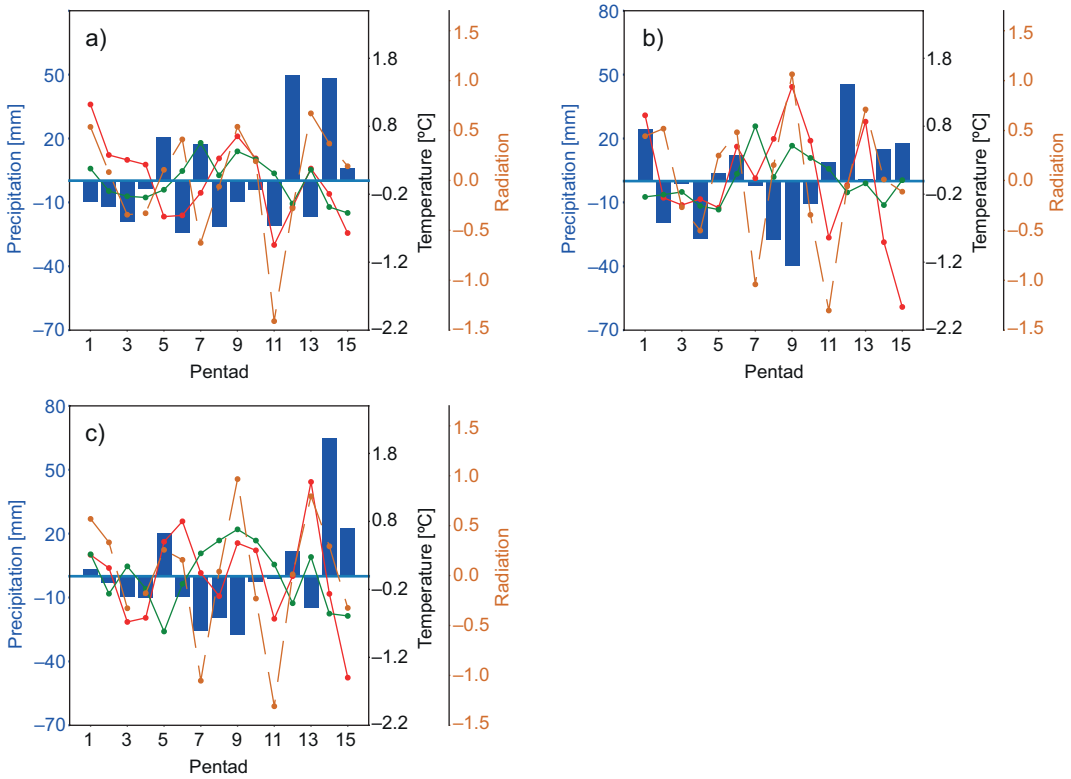

Fig. 8. Anomalies of the pentads estimated as the difference between the 5-day average and the mean of the study period for precipitation (blue bars), maximum and minimum temperature (red and green dotted lines, respectively), and surface incident shortwave radiation (dashed brown line) over (a) S1 (Gulf of Nicoya), (b) S3 (western Peninsula of Nicoya), and (c) S2 (central Peninsula of Nicoya).

5. Conclusions

This study focused on SB circulations over the Peninsula of Nicoya and the Gulf of Nicoya in northwestern Costa Rica, for the period from July 1 to September 16, 2004. The same study period as in Mora et al. (2020) but including more meteorological stations in that region. Using station data, the coastal evolution of SB under different synoptic conditions related to the intensity of the CLLJ was studied. It is confirmed that SB circulation appears in four of the studied stations (Pinilla, Guacalillo, Liberia, and Puntarenas). The main features found in these stations are summarized as follows.

Air temperature reached its minimum between 05:00 and 06:00 LST and maximum values near 12:00 and 13:00 LST. Precipitation peaks generally occur in the afternoon-night period (between 14:00 and 21:00 LST), showing a lag of about 4-6 h after the maximum temperature is reached, even in the case of Liberia, located over relatively plain terrain. SB onshore winds (with magnitudes greater than 4 m s^{-1}) were detected in the afternoon between 12:00 and 18:00 LST.

The SB inland penetration reaches about 20 km in a region characterized by relatively flat terrain. In Mora et al. (2020), there was no evidence of an SB system penetrating more than 25 km inland, as observed using a profile of meteorological station data from the Gulf of Nicoya into the Central Valley of Costa Rica, implying little or no connection with the convective activity and precipitation in that region. This feature contrasts with what is observed in Liberia regarding the inland incursion of the SB front and the associated observed precipitation distribution in the afternoons, 1 h or so after reaching the daily maximum temperature contrast. During night and dawn, offshore winds are weak due to the cooling of the land surface and probably mesoscale winds descending from the mountain chain to the east.

Regarding the spatial variability of the SB characteristics, the diurnal precipitation distribution is quite similar across the region of study, with maxima in the mid-afternoon. The inland penetration, however, is greater in the northern part of the PN mainly due to the flatness of the terrain.

During non-SBd, two different wind circulations were found: one related to strong northeasterly synoptic flow dominating the region, during the appearance of the MSD and enhanced CLLJ conditions. The second type of circulation is associated with predominant southwesterly synoptic forcing due to tropical disturbances or the transit of tropical waves from the Caribbean Sea. These results indicate that the CLLJ does not clearly modulate the onset and intensity of the registered SB events because it is weak (approximately –12 m s^{-1}) during the daytime hours in this region, while local effects seem to play a more relevant role.

The influence of the CLLJ in the SBd over the Pacific coast of Costa Rica is detected as a change of direction of the u10, however, wind-topography interaction may be an important process that could change the low-level wind direction over the slopes, as shown by Mora et al. (2020), although more observations combined with numerical model experiments are needed to demonstrate this interaction.

The algorithm used is considered to have a good ability to detect the SB and its spatiotemporal characteristics despite the SST data not having the desired spatial resolution. The daily precipitation patterns at the stations showed convective activity and precipitation in the afternoon hours, consistent with a typical SB circulation. The results are encouraging for future research, as the region is of great importance to the country's economy due to its artisanal fishing, agriculture, and tourism, the most important socio-economic activities in the area. Furthermore, the analyzed region includes the two most important ports in the country on the Pacific, serving as points of arrival and departure for tourist cruises and industrial ships that negatively impact air quality.

Acknowledgments

Costa Rica's National Meteorological Institute (IMN by its Spanish acronym) provided the meteorological station data used in this work. The authors wish to acknowledge the support of the projects VI-805-A4-906/B9-454/B8-604/C3-079/C3-991 from the Center for Geophysical Research of the University of Costa Rica (UCR). The authors would like to thank Paula Marcela Pérez Briceño for her assistance with Figure 1 and Allan Chinchilla Arias for providing the area of the PN used herein. The Ticosonde/NAME program was possible through support from the Earth Science Enterprise at NASA, the NOAA Office for Global Programs, the IMN, UCR (CIGEFI and School of Physics), Universidad Nacional (UNA), Centro Nacional de Alta Tecnología (CeNAT), and Comité Regional de Recursos Hidráulicos (CRRH).

References

Abbs DJ. 1986. Sea-breeze interactions along a concave coastline in Southern Australia: Observations and numerical modeling study. Monthly Weather Review 114: 831-848. https://doi.org/10.1175/1520-0493(1986)114<0831:SBIAAC>2.0.CO;2

Abel MR, Hall A, Fovell RG. 2007. Dynamical controls on the diurnal cycle of temperature in complex topography. Climate Dynamics 29: 277-292. https://doi.org/10.1007/s00382-007-0239-8

Allende-Arandía ME, Zavala-Hidalgo J, Torres-Freyermuth A, Appendini CM, Cerezo-Mota R, Taylor-Espinosa N. 2020. Sea-land breeze diurnal component and its interaction with a cold front on the coast of Sisal, Yucatan: A case study. Atmospheric Research 244: 105051. https://doi.org/10.1016/j.atmosres.2020.105051

Alms V, Wolff M. 2019. The Gulf of Nicoya (Costa Rica) fisheries system: Two decades of change. Marine and Coastal Fisheries 11: 139-161. https://doi.org/10.1002/mcf2.10050

Amador JA. 2008. The Intra-Americas Sea low-level jet. Overview and future research. Annals of the New York Academy of Sciences 1146: 153-188. https://doi.org/10.1196/annals.1446.012

Amador JA, Durán-Quesada AM, Rivera ER, Mora G, Sáenz F, Calderón B, Mora N. 2016. The easternmost tropical Pacific. Part II: Seasonal and intraseasonal modes of atmospheric variability. Revista de Biología Tropical 64: S23-S57. https://doi.org/10.15517/rbt.v64i1.23409

Amador JA, Anderson MJ, Calderón B, Pribyl K. 2018. The October 1891 Cartago (Costa Rica) floods from documentary sources and 20CR data. International Journal of Climatology 38: 4830-4845. https://doi.org/10.1002/joc.5701

Amador JA, Arce-Fernández D. 2022. WWLLN Hot and cold-spots of lightning activity and their relation to climate in an extended Central America region 2012-2020. Atmosphere 13: 76. https://doi.org/10.3390/atmos13010076

Anjos M, Lopes A. 2019. Sea breeze front identification on the northeastern coast of Brazil and its implications for meteorological conditions in the Sergipe region. Theoretical and Applied Climatology 137: 2151-2165. https://doi.org/10.1007/s00704-018-2732-x

Azorin-Molina C, Chen D. 2009. A climatological study of the influence of synoptic-scale flows on sea breeze evolution in the Bay of Alicante (Spain). Theoretical and Applied Climatology 96: 249-260. https://doi.org/10.1007/s00704-008-0028-2

Azorin-Molina C, Tijm S, Chen D. 2011. Development of selection algorithms and databases for sea breeze studies. Theoretical and Applied Climatology 106: 531-546. https://doi.org/10.1007/s00704-011-0454-4

Castro-Campos MV, Jiménez-Ramón JA. 2021. Atlas marino-costero del Golfo de Nicoya, Costa Rica. Fundación MarViva, San José, Costa Rica. Available at https://marviva.net/wp-content/uploads/2022/05/Atlas-Golfo-Nicoya-web.pdf (accessed 2023 January 23)

Cook KH, Vizy EK. 2010. Hydrodynamics of the Caribbean low-level jet and Its relationship to precipitation. Journal of Climate 23: 1477-1494. https://doi.org/10.1175/2009JCLI3210.1

Curtis S. 2004. Diurnal cycle of rainfall and surface winds and the mid-summer drought of Mexico/Central America. Climate Research 27: 1-8. https://doi.org/10.3354/cr027001

Davis SR, Farrar JT, Weller RA, Jiang H, Pratt LJ. 2019. The land-sea breeze of the Red Sea: Observations, simulations, and relationships to regional moisture transport. Journal of Geophysical Research: Atmospheres 124: 13803-13825. https://doi.org/10.1029/2019JD031007

Di Bernardino A, Iannarelli AM, Casadio S, Mevi G, Campanelli M, Casasanta G, Cede A, Tiefengraber M, Siani AM, Spinei E, Cacciani M. 2021. On the effect of sea breeze regime on aerosols and gases properties in the urban area of Rome, Italy. Urban Climate 37: 100842. https://doi.org/10.1016/j.uclim.2021.100842

Drobinski P, Rotunno R, Dubos T. 2011. Linear theory of the sea breeze in a thermal wind. Quarterly Journal of the Royal Meteorological Society 137: 1602-1609. https://doi.org/10.1002/qj.847

Estoque MA. 1961. A theoretical investigation of the sea breeze. Quarterly Journal of the Royal Meteorological Society 87: 136-146. https://doi.org/10.1002/qj.49708737203

Estoque MA. 1962. The sea breeze as a function of the prevailing synoptic situation. Journal of the Atmospheric Sciences 19: 244-250. https://doi.org/10.1175/1520-0469(1962)019<0244:TSBAAF>2.0.CO;2

Gille ST, Llewellyn Smith SG, Lee SM. 2003. Measuring the sea breeze from QuikSCAT scatterometry. Geophysical Research Letters 30: 14. https://doi.org/10.1029/2002GL016230

Gille ST, Llewellyn Smith SG, Statom NM. 2005. Global observations of the land breeze. Geophysical Research Letters 32: L05605. https://doi.org/10.1029/2004GL022139

Gouirand I, Moron V, Sing B. 2020. Seasonal atmospheric transitions in the Caribbean basin and Central America. Climate Dynamics 55: 1809-1828. https://doi.org/10.1007/s00382-020-05356-6

He J, Chen D, Gu Y, Jia H, Zhong K, Kang Y. 2022. Evaluation of planetary boundary layer schemes in WRF model for simulating sea-land breeze in Shanghai, China. Atmospheric Research 278: 106337. https://doi.org/10.1016/j.atmosres.2022.106337

Hersbach H, Bell B, Berrisford P, Hirahara S, Horányi A, Muñoz-Sabater J, Nicolas J, Peubey C, Radu R, Schepers D, Simmons A, Soci C, Abdalla S, Abellan X, Balsamo G, Bechtold P, Biavati G, Bidlot J, Bonavita M, De Chiara G, Dahlgren P, Dee D, Diamantakis M, Dragani R, Flemming J, Forbes R, Fuentes M, Geer A, Haimberger L, Healy S, Hogan RJ, Hólm E, Janisková M, Keeley S, Laloyaux P, López P, Lupu C, Radnoti G, de Rosnay P, Rozum I, Vamborg F, Villaume S, Thépaut J-N. 2020. The ERA5 global reanalysis. Quarterly Journal of the Royal Meteorological Society 146: 1999-2049. https://doi.org/10.1002/qj.3803

Hoyos I, Domínguez F, Cañón-Barriga J, Martínez JA, Nieto R, Gimeno L, Dirmeyer PA. 2018. Moisture origin and transport processes in Colombia, northern South America. Climate Dynamics 50: 971-990. https://doi.org/10.1007/s00382-017-3653-6

IMN-MINAE. 2004. Boletín Meteorológico Mensual 27(9): 1-25, Costa Rica.

Intrieri JM, Little CG, Shaw WJ, Banta RM, Durkee PA, Hardesty RM. 1990. The Land/Sea Breeze Experiment (LASBEX). Bulletin of the American Meteorological Society 71: 656-664. https://doi.org/10.1175/1520-0477-71.5.656

Karlsson KG, Anttila K, Trentmann J, Stengel M, Fokke Meirink J, Devasthale A, Hanschmann T, Kothe S, Jääskeläinen E, Sedlar J, Benas N, van Zadelhoff GJ, Schlundt C, Stein D, Finkensieper S, Håkansson N, Hollmann R. 2017. CLARA-A2: The second edition of the CM SAF cloud and radiation data record from 34 years of global AVHRR data. Atmospheric Chemistry and Physics 17: 5809-5828. https://doi.org/10.5194/acp-17-5809-2017

Li J, Pan Y, Li Q, Lenschow DH, Zhou M, Xiao X, Wang Y, Cheng Z. 2023. Observational analyses of a penetrating sea-breeze front in the Beijing-Tianjin-Hebei urban agglomeration. Urban Climate 47: 101353. https://doi.org/10.1016/j.uclim.2022.101353

Lizano OG, Amador-A J, Soto R. 2001. Caracterización de manglares de Centroamérica con sensores remotos. Revista de Biología Tropical 49: 331-340.

Ma Y, Xin J, Zhang X, Dai L, Schaefer K, Wang S, Wang Y, Wang Z, Wu F, Wu X, Fan G. 2021. Land-sea breeze circulation structure on the west coast of the Yellow Sea, China. Atmospheric and Oceanic Science Letters 14: 100003. https://doi.org/10.1016/j.aosl.2020.100003

Madrigal-Leer F, Martínez-Montandón A, Solís-Umaña M, Helo-Guzmán F, Alfaro-Salas K, Barrientos-Calvo I, Camacho-Mora Z, Jiménez-Porras V, Estrada-Montero S, Morales-Martínez F. 2020. Clinical, functional, mental and social profile of the Nicoya Peninsula centenarians, Costa Rica, 2017. Aging Clinical and Experimental Research 32: 313-321. https://doi.org/10.1007/s40520-019-01176-9

Magaña V, Amador JA, Medina S. 1999. The midsummer drought over Mexico and Central America. Journal of Climate 12: 1577-1588. https://doi.org/10.1175/1520-0442(1999)012<1577:TMDOMA>2.0.CO;2

Maldonado T, Rutgersson A, Alfaro E, Amador JA, Claremar B. 2016. Interannual variability of the midsummer drought in Central America and the connection with sea surface temperatures. Advances in Geosciences 42: 35-50. https://doi.org/10.5194/adgeo-42-35-2016

Mapes BE, Warner TT, Xu M, Negri AJ. 2003a. Diurnal patterns of rainfall in northwestern South America. Part I: Observations and context. Monthly Weather Review 131: 799-812. https://doi.org/10.1175/1520-0493(2003)131<0799:DPORIN>2.0.CO;2

Mapes BE, Warner TT, Xu M. 2003b. Diurnal patterns of rainfall in northwestern South America. Part III: Diurnal gravity waves and nocturnal convection offshore. Monthly Weather Review 131: 830-844. https://doi.org/10.1175/1520-0493(2003)131<0830:DPORIN>2.0.CO;2

Masouleh ZP, Walker DJ, McCauley Crowther J. 2019. A long-term study of sea-breeze characteristics: A case study of the coastal city of Adelaide. Journal of Applied Meteorology and Climatology 58: 385-400. https://doi.org/10.1175/JAMC-D-17-0251.1

Merchant CJ, Embury O, Bulgin CE, Block T, Corlett GK, Fiedler E, Good SA, Mittaz J, Rayner NA, Berry D, Eastwood S, Taylor M, Tsushima Y, Waterfall A, Wilson R, Donlon C. 2019. Satellite-based time-series of sea-surface temperature since 1981 for climate applications. Scientific Data 6: 223. https://doi.org/10.1038/s41597-019-0236-x

Mitsumoto S, Ueda H, Ozoe H. 1983. A laboratory experiment on the dynamics of the land and sea breeze. Journal of the Atmospheric Sciences 40: 1228-1240. https://doi.org/10.1175/1520-0469(1983)040<1228:ALEOTD>2.0.CO;2

Mora N, Amador JA, Rivera ER, Maldonado T. 2020. A sea breeze study during Ticosonde-NAME 2004 in the central Pacific of Costa Rica: Observations and numerical modeling. Atmosphere 11: 1333. https://doi.org/10.3390/atmos11121333

Muñoz E, Busalacchi AJ, Nigam S, Ruiz-Barradas A. 2008. Winter and summer structure of the Caribbean low-level jet. Journal of Climate 21: 1260-1276. https://doi.org/10.1175/2007JCLI1855.1

Neumann J, Mahrer Y. 1971. A theoretical study of the land and sea breeze circulation. Journal of the Atmospheric Sciences 28: 532-542. https://doi.org/10.1175/1520-0469(1971)028<0532:ATSOTL>2.0.CO;2

Pérez RA, Ortiz RJC, Bejarano ALF, Otero DL, Restrepo LJC, Franco HA. 2018. Sea breeze in the Colombian Caribbean coast. Atmósfera 31: 389-406. https://doi.org/10.20937/ATM.2018.31.04.06

Physick WL, Smith RK. 1985. Observations and dynamics of sea-breezes in northern Australia. Australian Meteorological Magazine 33: 51-63.

Qian T, Epifanio CC, Zhang F. 2009. Linear theory calculations for the sea breeze in a background wind: The equatorial case. Journal of the Atmospheric Sciences 66: 1749-1763. https://doi.org/10.1175/2008JAS2851.1

Rafiq S, Pattiaratchi C, Janeković I. 2020. Dynamics of the land-sea breeze system and the surface current response in south-west Australia. Journal of Marine Science and Engineering 8: 931. https://doi.org/10.3390/jmse8110931

Ramírez P. 1983. Estudio meteorológico de los veranillos en Costa Rica. Nota de investigación #5. Instituto Meteorológico Nacional y Ministerio de Agricultura y Ganadería, San José, Costa Rica. Available at https://www.imn.ac.cr/documents/10179/20909/Estudio+sobre+veranillos+en+Costa+Rica (accessed 2024 January 08)

Reddy TVR, Mehta SK, Ananthavel A, Ali S, Annamalai V, Rao DN. 2021. Seasonal characteristics of sea breeze and thermal internal boundary layer over Indian east coast region. Meteorology and Atmospheric Physics 133: 217-232. https://doi.org/10.1007/s00703-020-00746-1

Reddy BR, Srinivas CV, Venkatraman B. 2022. Observational analysis and numerical simulation of sea breeze using WRF model over the Indian southeast coastal region. Meteorology and Atmospheric Physics 134: 57. https://doi.org/10.1007/s00703-022-00891-9

Reddy BR, Srinivas CV, Venkatraman B. 2023. Impact of sea-breeze circulation on the characteristics of convective thunderstorms over southeast India. Meteorology and Atmospheric Physics 135: 5. https://doi.org/10.1007/s00703-022-00941-2

Román-Cascón C, Mulero-Martínez R, Bruno M, Izquierdo A, Yagüe C, Álvarez O, Gómez-Enri J, Mañanes R, Adame JA. 2022. Coastal-breeze simulation with the WRF model: Analysing the sensitivity to land/sea surface temperature changes. EMS Annual Meeting Abstracts 19: EMS2022-199. Bonn, Germany, 5-9 September. https://doi.org/10.5194/ems2022-199

Van Rossum G, Drake, FL. 2009. Python 3 reference manual. CreateSpace, Scotts Valley, CA.

Whelan T. 1989. Environmental contamination in the Gulf of Nicoya, Costa Rica. Ambio 18: 302-304.

Wiggins RM, Lintner BR, Serra YL, Durán-Quesada AM, Garbanzo-Salas M, Hernández-Deckers D, Torri G. 2023. Tropical easterly waves over Costa Rica and their relationship to the diurnal cycle of rainfall. Geophysical Research Letters 50: e2023GL104159. https://doi.org/10.1029/2023GL104159

Zárate-Hernández E. 1977. Principales sistemas de vientos que afectan a Costa Rica y sus relaciones con la precipitación. B.Sc. thesis. Universidad de Costa Rica.